

Concise whole-cell modeling of BK_{Ca} CaV activity controlled by local coupling and stoichiometry

Francesco Montefusco¹, Alessia Tagliavini¹, Marco Ferrante², and Morten Gram Pedersen ^{*1}

¹Department of Information Engineering, University of Padua, 35131 Padua, Italy

²Department of Mathematics "Tullio Levi-Civita", University of Padua, 35121 Padua, Italy

Abstract

Large-conductance Ca^{2+} -dependent K^+ (BK_{Ca}) channels are important regulators of electrical activity. These channels colocalize and form ion channel complexes with voltage-dependent Ca^{2+} (CaV) channels. Recent stochastic simulations of the BK_{Ca} -CaV complex with 1:1 stoichiometry have given important insight into the local control of BK_{Ca} channels by fluctuating nanodomains of Ca^{2+} . However, such Monte Carlo simulations are computationally expensive, and are therefore not suitable for large-scale simulations of cellular electrical activity. In this work we extend the stochastic model to more realistic BK_{Ca} -CaV complexes with 1: n stoichiometry, and analyze the single-complex model with Markov chain theory. From the description of a single BK_{Ca} -CaV complex, using arguments based on time-scale analysis, we derive a concise model of whole-cell BK_{Ca} currents, which can readily be analyzed and inserted into models of cellular electrical activity. We illustrate the usefulness of our results by inserting our BK_{Ca} description into previously published whole-cell models, and perform simulations of electrical activity in various cell types, which show that BK_{Ca} -CaV stoichiometry can affect whole-cell behavior substantially. Our work provides a simple formulation for the whole-cell BK_{Ca} current that respects local interactions in BK_{Ca} -CaV complexes, and indicates how local-global coupling of ion channels may affect cell behavior.

Keywords: Ion channel complex | Mathematical modeling | Electrical activity

Introduction

Mathematical modeling has played an important role in investigations of cellular electrophysiology at least since the works on neuronal action potential generation of Hodgkin and Huxley (1). In the Hodgkin-Huxley model and most of its descendants, the system of ion channels is coupled globally via the membrane potential or the bulk cytosolic Ca^{2+} concentration. However, some ion channels are colocalized, implying that the activity of one channel may affect the other via local control. Electrical activity is thus a result of the complex interactions of local and global coupling of ion channels. Of note, the standard Hodgkin-Huxley formulation does not take into account local coupling of channels.

*corresponding author; e-mail: pedersen@dei.unipd.it

Large-conductance Ca^{2+} - and voltage-dependent K^+ (BK_{Ca} , KCa1.1) channels, ubiquitously found in excitable cells where they shape electrical activity (2), provide an example of such ion channels, whose activity is influenced locally by associated voltage-gated Ca^{2+} channels (CaVs). BK_{Ca} channels have a single-channel conductance of ~ 100 pS in physiological conditions (3), and are activated by Ca^{2+} and transmembrane voltage, which is seen as a Ca^{2+} dependent left-shift of the BK_{Ca} activation curve (4–6). In neurons (7–10) and vascular myocytes (11), BK_{Ca} channels colocalize with CaVs, which exposes the BK_{Ca} channels to the Ca^{2+} nanodomains below the mouth of the CaV channels (12–15), where the local Ca^{2+} concentration reaches the tens of μM that are required for activating the BK_{Ca} channels at physiological voltages (2, 16). There is increasing evidence for a direct coupling between BK_{Ca} and CaV channels, forming BK_{Ca} -CaV ion channel complexes with a stoichiometry of 1-4 CaV channels per BK_{Ca} channel (2, 11), and differences in stoichiometry likely affect channel activity. Intuitively, we expect that more CaVs per complex would augment the BK_{Ca} open probability, both because of higher local Ca^{2+} concentration when the CaVs open simultaneously, and because of greater probability that at least one of the CaVs are open at any given time.

Recently, Cox (17) presented a Markov chain model for a BK_{Ca} -CaV complex with 1:1 stoichiometry, and performed Monte Carlo simulations that provided important insight into the open probability of BK_{Ca} channels during depolarizations and action potentials, and how e.g. inactivation of CaVs directly influence BK_{Ca} channel activity. Such Monte Carlo simulations are computationally intensive and explicit mathematical relations between assumptions and consequences are not available. Monte Carlo simulations have also been performed for whole-cell simulations of electrical activity to investigate the effects of stochastic ion channel kinetics, for example for Ca^{2+} -sensitive SK and BK_{Ca} channels controlled by local Ca^{2+} dynamics (18, 19). When stochasticity is not of interest, to speed up simulations, many models of whole-cell electrical activity that include BK_{Ca} channels express this current in a simplified way that neglects local effects due to the BK_{Ca} -CaV complexes (20, 21) or use heuristic expressions involving the whole-cell Ca^{2+} currents (22, 23), which may not respect the dynamics within BK_{Ca} -CaV complexes. Alternatively, diffusion of Ca^{2+} around a CaV (or a cluster of synchronized CaVs) has been simulated to investigate e.g. how BK channels inherit properties of the CaVs, and how distance between channels influence BK_{Ca} activity (10). Another frequent approach, which however neglects local interactions, is to model Ca^{2+} dynamics in one or more shells beneath the cell membrane, which then drives BK_{Ca} channels (24–26). The computational intensity is increased in such model since local Ca^{2+} concentrations resulting from buffering and diffusion must be simulated in addition to ion channel gating.

It would therefore be advantageous to have a simple but mechanistically correct model of the BK_{Ca} current, which respects the local effects of BK_{Ca} -CaV coupling, and that can be inserted in Hodgkin-Huxley-type models of whole-cell electrical activity. Such a model would also make explicit how local effects and stochastic ion channel kinetics are reflected in average, whole-cell behavior of BK_{Ca} channels with the advantage compared to simulations that the dependence on parameters can be read directly from the formulas of the reduced model. Here we achieve both these aims. Our approach is similar to analyses of Ca^{2+} -dependent inactivation of Ca^{2+} channels (27), and local control of ryanodine receptors in dyadic subspaces (28, 29). Importantly, in the nanodomains controlling BK_{Ca} activity, Ca^{2+} is fast enough to avoid the need for, e.g., a probability-density approach for handling local Ca^{2+} dynamics correctly at the whole-cell level (30). We use the mechanistically correct description of single BK_{Ca} -CaV complexes with 1:1 stoichiometry developed by Cox (17) as the natural starting point for constructing a reduced

model for BK_{Ca}-CaV complexes with 1:*n* stoichiometry to be inserted in whole-cell model of electrical activity. Our results give insight into the simulations of single BK_{Ca}-CaV complexes, and clarify that it is the local effects of ion channel kinetics rather than stochasticity *per se* that determine whole-cell activity.

Methods

BK_{Ca} channel model

We describe the BK_{Ca} channel with a model of single-channel gating with two states (closed and open). Figure S1A in the Supporting Material (SM) shows a schematic representation of the model, where *X* corresponds to the closed state and *Y* to the open state. The mathematical description of BK_{Ca} voltage- and calcium-dependent activation is given by

$$\frac{dp_Y}{dt} = -k^- p_Y + k^+ (1 - p_Y) \quad (1)$$

where p_Y represents the open probability for the BK_{Ca} channel, and k^- and k^+ are the voltage and calcium-dependent rate constants. As shown in the SM, from relatively mild assumptions and experimental evidence, we can express these rates as

$$k^- = w^-(V) f^-(Ca), \quad (2)$$

$$k^+ = w^+(V) f^+(Ca), \quad (3)$$

where Ca denotes the Ca²⁺ concentration at the BK_{Ca} channels. At fixed Ca²⁺ levels, BK_{Ca} activation is well described by Boltzmann functions (6, 8, 16). Hence, we assume that the voltage-dependent rate constants, w^- , for the transition from the open to closed state, and w^+ , for the transition from the closed to open state, have the standard forms

$$w^-(V) = w_0^- e^{-w_{yx} V}, \quad (4)$$

$$w^+(V) = w_0^+ e^{-w_{xy} V}, \quad (5)$$

where w_0^- and w_0^+ are voltage-independent.

There is evidence that at fixed V , Ca²⁺ stabilizes the open state (4), i.e., f^- should decrease with Ca , and that > 1 Ca²⁺ ion is needed for BK_{Ca} activation, which is a sigmoidal function of the Ca²⁺ concentration (4, 16). The calcium-dependent relations are therefore modeled by

$$f^-(Ca) = 1 - \frac{Ca^{n_{yx}}}{K_{yx}^{n_{yx}} + Ca^{n_{yx}}} = \frac{1}{1 + \left(\frac{Ca}{K_{yx}}\right)^{n_{yx}}}, \quad (6)$$

$$f^+(Ca) = \frac{Ca^{n_{xy}}}{K_{xy}^{n_{xy}} + Ca^{n_{xy}}} = \frac{1}{1 + \left(\frac{K_{xy}}{Ca}\right)^{n_{xy}}}, \quad (7)$$

where K_{yx} and K_{xy} are the calcium affinities when the channel closes and opens, respectively, and n_{yx} and n_{xy} are the corresponding Hill coefficients. By using the relationships Eqs. 4–7, we get the following formulas for the equilibrium open fraction of BK_{Ca} channel activation, p_{Y_∞} , and

the corresponding time constant τ_{p_Y} :

$$p_{Y_\infty} = \frac{k^+}{k^- + k^+} = \frac{1}{1 - e^{-\frac{V-V_0}{S_0}}}, \quad (8)$$

$$\tau_{p_Y} = \frac{1}{k^- + k^+} = \frac{e^{w_{xy}V}}{w_0^+} \left(1 + \left(\frac{K_{xy}}{Ca} \right)^{n_{xy}} \right) \frac{1}{1 - e^{-\frac{V-V_0}{S_0}}}, \quad (9)$$

where

$$V_0 = \left(\log \frac{w_0^-}{w_0^+} + \log \left(1 + \left(\frac{K_{xy}}{Ca} \right)^{n_{xy}} \right) - \log \left(1 + \left(\frac{Ca}{K_{yx}} \right)^{n_{yx}} \right) \right) S_0, \quad (10)$$

$$S_0 = \frac{1}{w_{yx} - w_{xy}}. \quad (11)$$

We use global optimization to estimate the model parameters providing the best fit to the experimental data (17), consisting of BK_{Ca} open probabilities and time constants as functions of voltage, at different Ca²⁺ concentrations. In particular, we formulate an optimization problem to minimize the sum of the squared errors between the simulated responses produced by the model and the corresponding experimental data as

$$\min_{\theta} J = \sum_j \sum_i \left(p_{Y_{\infty_j}}(V_i) - \hat{p}_{Y_{\infty_j}}(V_i, \theta) \right)^2 + \left(\tau_{p_{Y_j}}(V_i) - \hat{\tau}_{p_{Y_j}}(V_i, \theta) \right)^2, \quad (12)$$

where θ is the set of model parameters, $p_{Y_{\infty_j}}(V_i)$ and $\tau_{p_{Y_j}}(V_i)$ are the experimental BK_{Ca} steady-state open fraction and corresponding time constant, respectively, at the given voltage V_i for the j -th experiment (corresponding to a given Ca²⁺ concentration). $\hat{p}_{Y_{\infty_j}}(V_i, \theta)$ and $\hat{\tau}_{p_{Y_j}}(V_i, \theta)$ are the simulated equilibrium open fraction of the BK_{Ca} channel and the corresponding time constant of the model, respectively, at the given V_i for the j -th experiment. For the optimization, we use a hybrid Genetic Algorithm (GA) (31) that combines the most well-known type of evolutionary algorithm with a local gradient-based algorithm (32). We use the function `ga` from the MATLABTM (Mathworks, Natick, MA, USA) Global Optimization Toolbox and `fmincon` from the MATLABTM Optimization Toolbox as the local algorithm. We repeat the hybrid GA algorithm several times and select the parameter set that gives the best fitting. Table S1 reports the optimal model parameters, and Figure S1B-G shows the fits to the data.

CaV channel model

We describe the calcium channel dynamics with the following model (27):

$$\frac{dc}{dt} = \beta o - \alpha c, \quad (13)$$

$$\frac{do}{dt} = \alpha c + \gamma b - (\beta + \delta) o, \quad (14)$$

$$b = 1 - c - o = 1 - h, \quad (15)$$

where c corresponds to the closed state, o to the open state and b to the inactivated (blocked) state of the calcium channel; h represents the fraction of Ca²⁺ channels not inactivated, δ the rate for

channel inactivation and γ the reverse reactivation rate; α and β represent the voltage-dependent Ca^{2+} channel opening rate and closing rate, respectively, and have the following forms

$$\alpha(V) = \alpha_0 e^{-\alpha_1 V}, \quad (16)$$

$$\beta(V) = \rho \left(\beta_0 e^{-\beta_1 V} + \alpha_0 e^{-\alpha_1 V} \right). \quad (17)$$

As shown in (27), the processes of activation and inactivation can be approximately separated in time, since activation is much faster than inactivation. In particular, we achieve the following model for the activation variable, m_{CaV} ,

$$\frac{dm_{CaV}}{dt} = \frac{m_{CaV,\infty} - m_{CaV}}{\tau_{CaV}} \quad (18)$$

where

$$m_{CaV,\infty} = \frac{\alpha}{\alpha + \beta}, \quad \tau_{CaV} = \frac{1}{\alpha + \beta}, \quad (19)$$

and the following equation for inactivation

$$\frac{db}{dt} = m_{CaV,\infty} \delta - (m_{CaV,\infty} \delta + \gamma) b. \quad (20)$$

As for the BK_{Ca} channel, we use a global optimization method to optimize the parameters of Eqs. 16 and 17 to fit the experimental data presented by Cox (17), i.e., peak open probabilities and time constants as functions of voltage. For the values of $\gamma = 0.0020 \text{ ms}^{-1}$ and $\delta = 0.0025 \mu\text{M}^{-1} \text{ ms}^{-1} \times [Ca_{CaV}]$, we use those reported by Cox (17). Ca_{CaV} is the Ca^{2+} concentration at the internal mouth of the channel and defined by Eq. S1 in the SM with $r = 7 \text{ nm}$, representing the distance of the sensor for Ca^{2+} -dependent inactivation from the channel pore. Note that the relation given by Eq. 17 allows scaling of the amount of channel activation at high voltage values according to the experiments (i.e., not all the calcium channels are open even for high voltages). Table S1 reports the optimal parameters for the CaV activation model.

BK_{Ca} -CaV complex with 1:1 and 1:n stoichiometries

Combining the models for BK_{Ca} and CaV channels, we obtain the models of the 1:1 (see Results and Sections “Model of the 1:1 BK_{Ca} -CaV complex” and “Time-scale analysis and model simplifications” in the SM) and 1:n BK_{Ca} -CaV complexes (see Results and Section “Model for BK_{Ca} activation in complexes with k non-inactivated CaVs and its approximation” in the SM). Ca^{2+} levels sensed by the BK_{Ca} channel were assumed to reach steady-state immediately after CaV opening or closure (17), and the steady-state Ca^{2+} concentration Ca_o resulting from influx through a single CaV was calculated by an explicit formula (see Eq. S1 in the SM), assuming that CaV and BK_{Ca} channels are $r = 13 \text{ nm}$ apart (2, 9). At $V = 0 \text{ mV}$, $Ca_o \approx 19 \mu\text{M}$ (see Section “Model of the 1:1 BK_{Ca} -CaV complex” and Table S2 in the SM for further details). In the case of >1 CaV per complex, the linear buffer approximation (33) was used to summarize Ca^{2+} levels when more than one CaV is open. We note that $k_c^+ \approx 0$ (see Section “Model of the 1:1 BK_{Ca} -CaV complex” and Table S1 in the SM) since the background Ca^{2+} concentration Ca_c is much below the levels needed for BK_{Ca} activation at physiological voltages (2). Thus, a BK_{Ca} channel opens only when a CaV in the complex is open. This approximation is used widely in

our derivations, and is supported by the fact that Ca^{2+} influx via CaVs is needed to open BK_{Ca} channels (34), and that the submembrane Ca^{2+} concentration of some hundreds of nM that a BK_{Ca} in a complex without open CaVs would sense is too low to activate BK_{Ca} channels at physiological voltages (2, 17).

We refer to the SM for details on mathematical analysis of the time to first BK_{Ca} channel opening using phase-type distributions (35) (see Section “Model of the 1:1 BK_{Ca} -CaV complex” in the SM), and timescale analysis used for model reduction borrowing ideas from enzyme kinetics (36) (Sections “Time-scale analysis and model simplifications” and “Model for BK_{Ca} activation in complexes with k non-inactivated CaVs and its approximation” in the SM), as well as for details on the whole-cell models investigated (Section “Whole-cell models” in the SM).

Availability of models and computer code

MATLAB code containing the files for generating the results presented in the main text and Supporting Material is provided as an additional Supporting File S1.

Results

A simple Markov chain model of the BK_{Ca} -CaV complex

Cox (17) presented a stochastic model of a single CaV2.1 (P/Q-type) controlling a BK_{Ca} channel (α subunits only) via local Ca^{2+} . The channels were located 13 nm apart, corresponding to physical coupling (2, 9). The CaV was described by a 7-state Markov chain, and when the Ca^{2+} channel opened or closed, the local Ca^{2+} level was assumed to reach equilibrium instantaneously, in accordance with simulations of Ca^{2+} diffusion (12, 13, 17). The calculated local Ca^{2+} concentration was then assumed to drive a 10-state Markov chain model of the BK_{Ca} channel, and Monte Carlo simulations were performed.

We set out to simplify the description of the 7×10 -state Markov chain model of the BK_{Ca} -CaV complex. This was achieved by assuming a 3-state model for CaV (27) with states closed (C), open (O), or inactivated (B , for "blocked") (see Methods). Parameters were adjusted to reproduce traces from Cox (17). The BK_{Ca} channel was represented by a model with only 2 states, closed (X) or open (Y) (see Methods). The transitions between states were supposed to depend on voltage and local Ca^{2+} , which was assumed to reach equilibrium instantaneously, and depend on voltage via the single-channel Ca^{2+} current (17). Parameters describing BK_{Ca} kinetics were fitted to data from Cox (17). Combining these two models, we obtain a 6-state model of the BK_{Ca} -CaV complex (Figure 1A) that shows behavior similar to the 70-state model used by Cox (17) (Figure 1BC). Our simplified BK_{Ca} model does not describe details of single-channel kinetics, which is not our scope here, but reproduces satisfactorily activation curves and times (Figure S1), as well as whole-cell currents (Figures S4 and S5), thus making it appropriate for analysis of whole-cell BK_{Ca} activity.

Time to first opening

Interestingly, Cox (17) found that not all simulated BK_{Ca} channels open during 20 ms depolarizations or imposed action potentials. We now study the time to the first opening of the BK_{Ca} channel during a depolarization, which mathematically corresponds to the first time the Markov

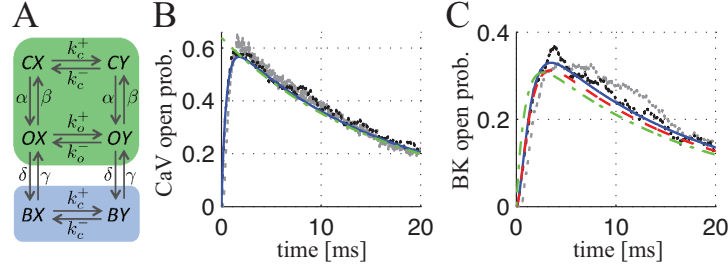


Figure 1: **A 6-state model of the BK_{Ca} -CaV complex with 1:1 stoichiometry and its simplification.** (A) Scheme indicating the 6 states and voltage-dependent transitions. C , O , and B refer respectively to closed, open, and inactivated states of the CaV, whereas X and Y indicate the closed and open states of the BK_{Ca} channel. The subscripts o and c on the horizontal transition rates indicate dependence on the Ca^{2+} concentration below an open, respectively closed, Ca^{2+} channel. At physiological voltages, the transition to a state with an open BK_{Ca} channel occurs virtually only when the CaV is open ($k_c^+ \approx 0$). The green box indicates states with non-inactivated CaVs, whereas the blue box highlights states with inactivated CaVs. The transitions between the colored boxes are slow compared to transitions within boxes. (B) Simulated CaV open probabilities in response to a voltage step from -80 mV to 0 mV, obtained from the 7-state Markov chain model (gray; (17)), the 3-state Markov chain model C, O, B (black; (27)), the ODE model corresponding to the 3-state model (Eqs. 13–15; blue), and the corresponding model assuming instantaneous activation $m_{CaV} = m_{CaV,\infty}$ (Eq. 20; dash-dotted green). (C) Simulated open probabilities, in response to a voltage step from -80 mV to 0 mV, for BK_{Ca} channels controlled by CaVs in complexes with 1:1 stoichiometry, obtained from the original 70-state Markov chain model (gray; (17)), the 6-state Markov chain model (panel A; black), the ODE model corresponding to the 6-state model (Eqs. S6–S11; blue), the simplified Hodgkin-Huxley-type model (Eq. 25; dashed red), and the corresponding model assuming instantaneous activation $m_{CaV} = m_{CaV,\infty}$ (dash-dotted green; see main text). In panels B and C, 1000 realizations were simulated for the Markov chain models, and the average of these Monte Carlo simulations are shown.

Chain Z corresponding to Figure 1A visits one of the states CY, OY or BY starting from state CX . We denote the time to first opening $T_{CX,Y}$, which is a random variable. Simulations show that eventually all BK_{Ca} channels open, and that the probability of channel opening before a given time t , $P(T_{CX,Y} < t)$, shows biphasic behavior (Figure S2). Taking advantage of the fact that transitions from CX to CY , and from BX to BY have virtually zero probability (BK_{Ca} channels open only if the CaV is open), we obtain explicit formulas for the average time to first opening $E(T_{CX,Y})$ and, more generally, for the distribution function $P(T_{CX,Y} < t)$ using phase-type distribution results for Markov Chains (35) (see Section “Time to first opening and phase-type distributions” in the SM),

$$E(T_{CX,Y}) = \frac{1}{\alpha} + \frac{1}{k_o^+} + \frac{1}{k_o^+} \left(\frac{\beta}{\alpha} + \frac{\delta}{\gamma} \right), \quad (21)$$

$$P(T_{CX,Y} < t) = 1 - \sum_{\psi \in \{C,O,B\}} (\exp(t\bar{Q}))_{CX,\psi X}, \quad (22)$$

where \bar{Q} is the sub-transition rate matrix of Z corresponding to states $\{CX, OX, BX\}$. Thus, the average time to first opening is inversely related to the opening rates of the CaV and BK_{Ca} , and to the rate of reactivation following inactivation of the CaV. The involvement of these two processes explains the biphasic behavior, since escape from inactivation is much slower than channel opening. Eq. 22 states that $P(T_{CX,Y} < t)$ is 1 minus the probability of not having left $\{CX, OX, BX\}$ before t , and makes it explicit that $\sim 15\%$ of BK_{Ca} channels do not open during a 20 ms depolarization (17), since $P(T_{CX,Y} < 20 \text{ ms}) \approx 85\%$ with our parameters (Figure S2).

A concise deterministic model of cellular BK_{Ca} activity derived from multiscale principles

1:1 stoichiometry

For Hodgkin-Huxley-type whole-cell simulations, we do not need to know the state of each single BK_{Ca} channel, but it suffices to follow the BK_{Ca} open probability p_Y over time, since in the presence of many channels the whole-cell BK_{Ca} current is $I_{BK} = g_{BK} p_Y (V - V_K)$, where g_{BK} is the maximal whole-cell BK_{Ca} conductance and V_K is the K^+ reversal potential.

The time evolution of the probability distribution of the Markov chain Z corresponding to the 6-state model in Figure 1A can be described by a system of 5 ordinary differential equations (ODEs) because the probabilities sum to 1. Denote, for $\psi \in \{C, O, B\}$ and $\xi \in \{X, Y\}$, the state probabilities $p_{\psi\xi}(t) = P(Z(t) = \psi\xi)$. Then $p_Y(t) = p_{CY}(t) + p_{OY}(t) + p_{BY}(t)$. As shown in Figure 1C, the average fraction of open channels calculated from Monte Carlo simulations of the Markov chain is well approximated by p_Y obtained from the ODE system.

Although the reduction to 5 ODEs for the description of the BK_{Ca} -CaV complexes is already a substantial reduction compared to Monte Carlo simulations, we wish to obtain an expression for the BK_{Ca} current of Hodgkin-Huxley form. Such a simplification provides further insight into the regulation of BK_{Ca} activity by CaVs, and provides the base for concise handling of BK_{Ca} -CaV complexes with 1: n stoichiometry.

We performed detailed time-scale analysis (see Section “Time-scale analysis and model simplifications” in the SM) based on the fact that re- and inactivation of CaVs are slower than (de-)activation. Thus, on a fast time scale, the average fraction of non-inactivated CaVs, $h =$

$1 - (p_{BX} + p_{BY})$, is assumed to be constant, and the model splits into two submodels with respectively 4 and 2 states (indicated by green and blue in Figure 1A).

In the system of ODEs describing the state probabilities of the corresponding reduced 4-state Markov chain (green in Figure 1A), it turns out that the dynamics of state CY is the fastest since CaV kinetics and BK_{Ca} -channel closure, when the CaV is closed, are faster reactions than BK_{Ca} gating in the presence of an open CaV (see Figure S3). Assuming quasi steady-state for CY , we derive a single ODE describing the gating variable m_{BK} , which models the fraction of open BK_{Ca} channels in complexes with non-inactivated CaV (see Section ‘‘Model simplification’’ in the SM),

$$\frac{dm_{BK}}{dt} = \frac{m_{BK,\infty} - m_{BK}}{\tau_{BK}}, \quad (23)$$

with steady-state and time constant given by

$$\begin{aligned} m_{BK,\infty} &= \frac{m_{CaV} k_o^+ (\alpha + \beta + k_c^-)}{(k_o^+ + k_o^-)(k_c^- + \alpha) + \beta k_c^-}, \\ \tau_{BK} &= \frac{\alpha + \beta + k_c^-}{(k_o^+ + k_o^-)(k_c^- + \alpha) + \beta k_c^-}. \end{aligned} \quad (24)$$

Here, m_{CaV} is defined by Eq. 18 and denotes the activation variable for the CaV in the complex, which is routinely characterized in patch clamp experiments and included in models of electrical activity via the time-constant, τ_{CaV} , and the steady-state activation function, $m_{CaV,\infty}$ (see Eq. 19). From these quantities, $\alpha = m_{CaV,\infty}/\tau_{CaV}$ and $\beta = 1/\tau_{CaV} - \alpha$ can be calculated. Note that Eq. 24 makes it explicit how $m_{BK,\infty}$ inherits properties of the associated Ca^{2+} channel type, as has been found experimentally (10, 37).

Now, since BK_{Ca} channels close rapidly in complexes with inactivated CaVs (blue in Figure 1A), we have $p_Y \approx m_{BK}h$. Thus, the BK_{Ca} current is approximated by the standard Hodgkin-Huxley expression

$$I_{BK} = g_{BK}m_{BK}h(V - V_K), \quad (25)$$

where m_{BK} is given by Eq. 23, and h is the inactivation function of the CaVs (see Eqs. 15 and 20). As shown in Figure 1C, the open-probability expression $m_{BK}h$ approximates the Monte Carlo simulations very well. From Eq. 25 it is evident that the BK_{Ca} channels in BK_{Ca} -CaV complexes exhibit inactivation because of inactivation of the associated CaVs, and with approximately identical dynamics, as found in experiments (8) and Monte Carlo simulations (Figure 1; (17)).

In many whole-cell models (e.g. (20–23)), the Ca^{2+} currents are assumed to activate instantaneously, which precludes calculation of α and β . Implicitly, such models assume that CaV gating is infinitely faster than the kinetics of other channels in the model. In our setting, this assumption corresponds to investigating the BK_{Ca} -CaV model defined by Eqs. 23–25 in the limit $\alpha, \beta \rightarrow \infty$. This leads to $\tau_{BK} \approx 1/[k_c^- - m_{CaV,\infty}(k_c^- - k_o^+ - k_o^-)]$ and $m_{BK,\infty} = k_o^+ m_{CaV,\infty} \tau_{BK}$, which are completely defined from BK_{Ca} kinetics and $m_{CaV,\infty}$. In combination with Eqs. 23 and 25, this model approximates the full system decently, except for the initial phase before CaV activation reaches equilibrium (Figure 1C, green). For whole-cell models neglecting CaV activation kinetics, this initial-phase error should be of no more concern than the error in the Ca^{2+} current resulting from the steady-state assumption for CaV activation (Figure 1B, green).

Complexes with multiple Ca^{2+} channels

As mentioned, a BK_{Ca} channel can bind up to 4 CaVs (2, 11). We extend our model to incorporate such cases, assuming that the n CaVs are all located 13 nm from the BK_{Ca} channel (2, 9, 17). Near the CaVs, the linear buffer approximation (33) holds, and the Ca^{2+} profile from n channels can be calculated by superimposing n nanodomains found for single, isolated CaVs.

One could in principle extend the Markov chain model in Figure 1A to a model with $3 \times n \times 2$ states. We take another approach to keep the model tractable. As discussed in the previous section, CaV inactivation is slow compared to other processes. We therefore assume that on a fast timescale, the fraction h of non-inactivated CaVs is constant, and note that the BK_{Ca} channel closes rapidly when all CaVs in the complex are inactivated.

Consider a BK_{Ca} -CaV complex with $k \in \{1, \dots, n\}$ non-inactivated CaVs. Neglecting inactivated CaVs, since they do not contribute to BK_{Ca} activation, such a complex can be described on the fast time scale by a Markov chain model with $2 \times (k + 1)$ states (Figure 2A). As for the case of 1:1 stoichiometry, we can approximate the dynamics of the BK_{Ca} open probability by a single ODE (see Section “Model for BK_{Ca} activation in complexes with k non-inactivated CaVs and its approximation” in the SM). Denote this open probability by $m_{\text{BK}}^{(k)}$, and note that $m_{\text{BK}}^{(1)} = m_{\text{BK}}$ in Eq. 23. Then

$$\frac{dm_{\text{BK}}^{(k)}}{dt} = \frac{m_{\text{BK},\infty}^{(k)} - m_{\text{BK}}^{(k)}}{\tau_{\text{BK}}^{(k)}}, \quad (26)$$

where $m_{\text{BK},\infty}^{(k)}$ and $\tau_{\text{BK}}^{(k)}$ are explicit functions of V , directly or via the local Ca^{2+} concentration (see Eq. S36 in the SM). The probability that k non-inactivated CaVs are present in a complex with n CaVs is $\binom{n}{k} h^k (1-h)^{n-k}$, and the whole-cell BK_{Ca} current is approximated by

$$I_{\text{BK}} = g_{\text{BK}} \sum_{k=1}^n \binom{n}{k} h^k (1-h)^{n-k} m_{\text{BK}}^{(k)} (V - V_K), \quad (27)$$

which involves n ODEs (Eq. 26) for the activations variables $m_{\text{BK}}^{(k)}$, and 1 ODE for h ($h = 1 - b$, where b is given by Eq. 20). As shown in Figure 2C, this expression provides a good approximation to the results from Monte Carlo simulations of the full Markov Chain. Note that if the CaVs do not inactivate, Eq. 27 reduces to

$$I_{\text{BK}} = g_{\text{BK}} m_{\text{BK}}^{(n)} (V - V_K). \quad (28)$$

We can now easily investigate how different stoichiometries of the BK_{Ca} -CaV complexes influence, e.g., activation of the BK_{Ca} channels. As expected, we find that the activation curve is shifted upwards as the number of CaVs per complex increase (Figure 2B, upper). Interestingly, a left-shift of the activation curve is seen when n increases. For example, with $n = 4$ CaVs per BK_{Ca} channel, BK_{Ca} activation is half-maximal at $V \approx -14$ mV, compared to $V \approx -5$ mV when $n = 1$, and half-maximal CaV activation at $V \approx -12$ mV. This result is due to the fact that the probability of at least one CaV being open is greater with more channels in the complex. For higher voltages, the single channel current decreases and the CaV open probability increases, with the result that, at strongly positive voltages, BK_{Ca} activation decays more gradually at $n = 1$ than for higher n . This difference is because the local Ca^{2+} level obtained with a single open CaV is insufficient for complete BK_{Ca} activation, and therefore the presence of more CaVs

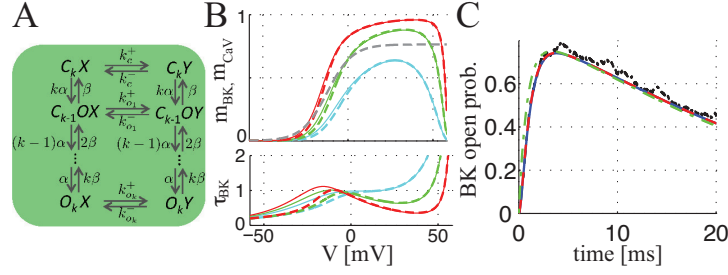


Figure 2: **Multiple CaVs per BK_{Ca}-CaV complex.** (A) Markov chain model for complexes with k non-inactivated CaVs. (B) Steady-state BK_{Ca} activation functions (upper) and time-constants (lower) for BK_{Ca} channels in complexes with 1 (cyan), 2 (green) or 4 (red) CaVs given from Eq. 26 (see Eq. S36 in the SM for the details; solid) or from the approximation defined by Eq. 29 (dashed). The grey dashed curve shows the CaV activation function $m_{CaV, \infty}$, for comparison. (C) Simulated BK_{Ca} open probabilities in response to a voltage step from -80 mV to 0 mV, obtained from Monte Carlo simulations of the Markov model of n inactivating independent CaVs controlling a BK_{Ca} channel (black), from the ODE model of all states in panel A coupled to CaV inactivation (Eqs. S19–S25 and Eq. 27; solid blue), from the reduced ODE model considering CaV activation kinetics (Eqs. 26 and 27; dashed red), and from the simplification assuming $m_{CaV} = m_{CaV, \infty}$ (Eqs. 29 and 27; dash-dotted green).

per complex becomes advantageous, since the CaVs may open simultaneously, leading to higher local Ca^{2+} levels. This interpretation also underlies the finding that BK_{Ca} activation is faster with higher n at positive voltages (Figure 2B, lower).

As mentioned above, many whole-cell models assume instantaneous activation of CaVs. This assumption implies that vertical transitions in Figure 2A are in quasi-equilibrium, and hence that e.g. $p_{C_i O_{k-i} Y} = \binom{k}{i} (1 - m_{CaV, \infty})^{k-i} m_{CaV, \infty}^i p_Y$, with notation as for the case of 1:1 stoichiometry. Then, $m_{BK}^{(k)}$ follows Eq. 26 with

$$\tau_{BK}^{(k)} = \left[\sum_{i=1}^k \binom{k}{i} (1 - m_{CaV, \infty})^{k-i} m_{CaV, \infty}^i (k_{o_i}^+ + k_{o_i}^-) + (1 - m_{CaV, \infty})^k k_c^- \right]^{-1}, \quad (29)$$

$$m_{BK, \infty}^{(k)} = \left[\sum_{i=1}^k \binom{k}{i} (1 - m_{CaV, \infty})^{k-i} m_{CaV, \infty}^i k_{o_i}^+ \right] \tau_{BK}^{(k)}.$$

This simplified expression provides decent fits to activation functions (Figure 2B, upper) and simulated currents (Figure 2C), and – in our experience – yields reliable results in whole-cell simulations for cells with relatively slow action potential dynamics, as shown below, in spite of a slight underestimation of $\tau_{BK}^{(k)}$ at negative voltages (Figure 2B, lower).

Whole-cell simulations of electrical activity shaped by BK_{Ca}-CaV complexes

We now illustrate the type of whole-cell modeling that can be performed readily with our Hodgkin-Huxley-type model of the BK_{Ca} current controlled locally by CaVs in BK_{Ca}-CaV complexes.

BK_{Ca}-CaV stoichiometry controls fAHP in a neuronal model

It is well established that in many neurons BK_{Ca} channels play an important role in action potential (AP) repolarization and fast after-hyperpolarization (fAHP), i.e., the undershoot seen after an AP (2, 38), which are important, e.g., for controlling firing frequency and transmitter release. We here adapt a model of AP generation and fAHP in hypothalamic neurosecretory cells (20) to investigate how BK_{Ca}-CaV complexes influence fAHP. In the original model, CaVs are assumed not to inactivate and to activate instantaneously. We modified the model to include CaV activation dynamics with time constant $\tau_{CaV} = 1.25$ ms (37, 39), and inserted our whole-cell BK_{Ca} model (Eq. 28) in place of the original representation of BK_{Ca} currents.

Our results suggest that more than one CaV channel is needed in the BK_{Ca}-CaV complex to develop fAHP that is reduced by BK_{Ca}-channel blockers (Figure 3A). The difference between 1:1 and 1: n BK_{Ca}-CaV stoichiometry is not a simple result of more BK_{Ca} conductance. Increasing the BK_{Ca} conductance 4-fold in the case of 1:1 stoichiometry, much more than the difference between the activation functions $m_{BK,\infty}^{(1)}$ and $m_{BK,\infty}^{(4)}$ (Figure 2B), leads to less fAHP than for 1:4 stoichiometry (Figure 3A, insert). Thus, differences in BK_{Ca} activation kinetics and the shapes of activation functions (Figure 2B) play a non-trivial role in shaping APs.

Different CaV types affect electrical activity differently in a model of human β -cell electrophysiology

In our recent model of electrical activity in human β -cells (22, 23), we modeled the BK_{Ca}-current heuristically. The BK_{Ca} open probability was proportional to the whole-cell Ca²⁺ current, and this expression was found to reasonably reproduce published data (40) regarding the BK_{Ca} activation function and the effects of BK_{Ca} block on AP firing (22).

We now assume that the BK_{Ca} channels form complexes with either T-, L-, or P/Q-type CaVs (22, 40), and vary the BK_{Ca}-CaV stoichiometry. As explained in greater details in the SM, the different types of CaV differ with respect to activation and inactivation properties, and whole-cell conductance (22, 23). The resulting BK_{Ca} model is then fit to experimental I-V data (40) (Figure S7), and inserted in the whole-cell model. T-type CaVs inactivate rapidly (22, 40), and do not activate much BK_{Ca} current during the relatively broad action potentials. For this reason, simulated BK_{Ca} block results in almost no increase in AP height (Figure 3B), in contrast to experiments (40).

In human β -cells, L-type Ca²⁺ channels show inactivation on a time-scale comparable to the duration of an AP (22, 40). When coupled to BK_{Ca} channels in the model, good fits to the BK_{Ca} I-V activation curve are obtained, but for different values of the maximal whole-cell BK_{Ca} conductance g_{BK} (Figure S7). In simulations of electrical activity, BK_{Ca} currents controlled by L-type CaVs reduce AP height, independently of the number of CaVs per complex (Figure 3C).

BK_{Ca}-CaV complexes with P/Q-type Ca²⁺ channels, which activate at very depolarized potentials and show very slow inactivation in human β -cells (22, 40), lead to BK_{Ca} currents that activate at slightly more depolarized potentials than in experiments, except for the case of 1:4 BK_{Ca}-CaV stoichiometry (Figure S7). Simulated application of a BK_{Ca} channel antagonist increases AP height ~ 15 mV, in good correspondence with experiments. Assuming fewer CaVs per complex, leads to poorer fit of the I-V curve and to less difference between APs obtained with operating and blocked BK_{Ca} channels (Figure 3D).

We conclude that AP firing is affected differently by BK_{Ca} currents depending on the CaV type

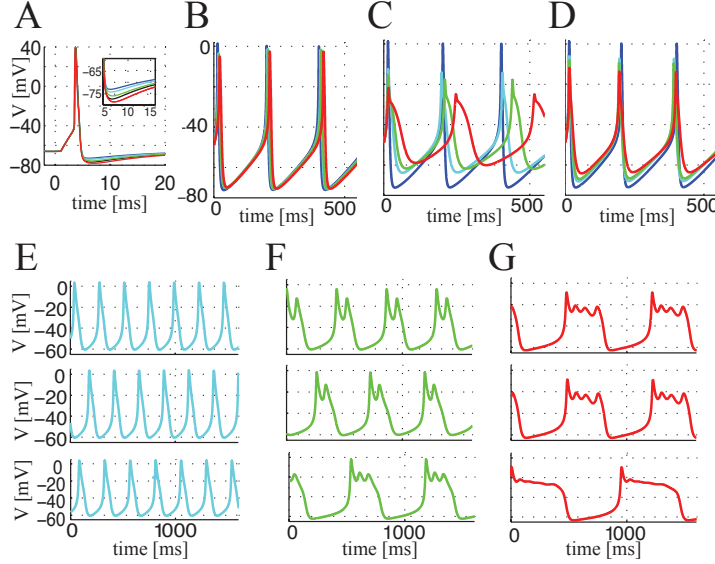


Figure 3: **Whole-cell simulations.** **(A)** Simulated AP in a neuronal model (20) with 1: n stoichiometry BK_{Ca} -CaV complexes with $n = 1$ (cyan), $n = 2$ (green) or $n = 4$ (red). The whole-cell BK_{Ca} current is described by Eq. 28 (i.e. BK_{Ca} coupled with non-inactivating CaVs), where the BK_{Ca} activation, $m_{BK}^{(n)}$, is modeled by Eq. 26 (see Eq. S36 in the SM for the details) and $g_{BK} = 1 \text{ mS cm}^{-2}$. The blue curve shows the case of BK_{Ca} block ($g_{BK} = 0 \text{ mS cm}^{-2}$), and the trace in black displays the result with $n = 1$, $g_{BK} = 4 \text{ mS cm}^{-2}$. The insert shows a zoom on the fAHP. **(B-D)** Simulated APs in a model of human β -cells (22) with BK_{Ca} channels located in complexes with n T-type (B), L-type (C), or P/Q-type (D) CaVs, with $n = 1, 2$ or 4. The whole-cell BK_{Ca} current is described by Eq. 27 (with inactivating T- and L-type CaVs) or Eq. 28 (with non-inactivating P/Q-type CaVs), where $m_{BK}^{(n)}$ is modeled by Eq. 29. Color coding as in panel A. **(E-G)** Simulated activity in a model of lactotrophs (21) with 1: n BK_{Ca} -CaV complexes with $n = 1$ (E), $n = 2$ (F), or $n = 4$ (G). The whole-cell BK_{Ca} current is described by Eq. 28, where $m_{BK}^{(n)}$ is modeled by the complete BK_{Ca} model with $2 \times (n+1)$ states (Figure 2A) described using Eqs. S19–S25 (upper traces), by Eq. 26 (middle traces), and by Eq. 29 (lower traces).

controlling BK_{Ca} activity, due to differences in activation and inactivation properties. Since BK_{Ca} block stimulates insulin secretion in human (40) and mouse (41) β -cells, a better understanding of the interaction between different types of CaVs and BK_{Ca} channels may provide novel insight into insulin release in health and disease.

Bursting behavior depends on BK_{Ca} -CaV stoichiometry in a model of pituitary cells

In pituitary cells BK_{Ca} channels have been found to be intimately involved in the genesis of so-called plateau bursting, which consists of a few small oscillations riding on a depolarized plateau, and is important for secretion (42, 43). We now investigate how BK_{Ca} -CaV properties affect such bursting activity in a model of electrical activity in pituitary lactotrophs (21). In this model a single Ca^{2+} -channel type is present, which is assumed to activate instantaneously and not to inactivate. The BK_{Ca} current was modeled as a purely voltage-dependent current, neglecting Ca^{2+} dependency (21). In place of this simplified representation, we substitute our concise BK_{Ca} model controlled by CaVs in complexes.

With 1:1 stoichiometry, spiking electrical activity is observed, since insufficient BK_{Ca} current is generated (Figure 3E). In contrast, with more than one CaV per complex, plateau bursting appears with the number of small oscillations per burst depending on the number of CaVs per BK_{Ca} -CaV complex (Figure 3FG). Although the quantitative behavior is independent of the approximation for $m_{BK}^{(n)}$, minor qualitative differences are present. The approximation given by Eq. 26 reproduces very well the behavior obtained from the complete model for the BK_{Ca} -CaV complex (Figure 3FG, upper and middle panels), whereas the further simplification given by Eq. 29 produces smaller and more spikes per burst. Nonetheless, considering parameter uncertainties and experimental variations, even Eq. 29 produces reliable results.

Discussion

Models of cellular electrical activity typically do not consider local control in ion channel complexes. This fact is probably to a large extent because of the large computational costs of detailed simulations of Markov chain models (17) or reaction-diffusion models (10) that consider single complexes. In contrast, in the field of Ca^{2+} modeling, global procedures that respect local mechanisms have been presented (28–30).

We here applied similar methods to the BK_{Ca} -CaV complex to obtain Hodgkin-Huxley representations of the BK_{Ca} current that correctly take local control into account. Importantly, in our approach the effects of ion channel colocalization are handled via a deterministic model representation by averaging the stochastic dynamics in single ion channel complexes appropriately. Our timescale analysis allowed us to handle scenarios with more than one CaV per BK_{Ca} -CaV complex, thus providing important insight into the role of channel stoichiometry. Treating such cases via direct stochastic simulations of the BK_{Ca} and CaV simulations would be computationally cumbersome, and would not provide the same kind of analytical understanding. For example, we found explicit expressions for the time to first opening of a BK_{Ca} channel, thus providing theoretical insight into simulation results (17). Our findings also highlighted that $n > 1$ CaV per complex left-shifts the BK_{Ca} activation curve, since the presence of more CaVs increase the probability that at least one CaV is open and activate the associated BK_{Ca} channel.

We illustrated the usefulness of our theoretical results by applying the concise representations of BK_{Ca} currents to previously published whole-cell models of electrical activity. We chose a model

of neuronal APs that has previously been used to investigate how BK_{Ca} channels contribute to fast after-hyperpolarization (fAHP) (20). The simulations based on our BK_{Ca} -CaV model suggest that the kinetics of BK_{Ca} activation, which depends on the number associated CaVs (Figure 2), influence fAHP generation. It would be interesting to investigate experimentally whether defect BK_{Ca} -CaV coupling underlies disturbances in fAHP generation, as predicted by the model. In *Xenopus* motor nerve terminals, BK_{Ca} -CaV coupling differs between the release face and the non-synaptic surface of varicosities (44), which in the light of our simulations may indicate spatial heterogeneity with respect to e.g. fAHP.

We went on to investigate how the activation and inactivation properties of specific types of Ca^{2+} channels assumed to be present in BK_{Ca} -CaV complexes influence whole-cell electrical activity in a model of human β -cells (22). Since both coupling of BK_{Ca} channels to L- and P/Q-type CaVs, and different stoichiometries of the complexes, allow for simulations comparable to experiments, our findings do not allow us to conclude on the structure of BK_{Ca} -CaV complexes in human β -cells. Further insight into the control by CaVs of BK_{Ca} channels, which are involved in regulation of insulin release (40, 41), may lead to a better understanding of β -cell function and how it becomes disturbed in diabetes.

Finally, a model of pituitary cells (21) was used to study the role of BK_{Ca} channels in the generation of plateau bursting, which is important for secretion of pituitary hormones (42). We found that a reduced number of CaVs per complex, for example because of disturbed BK_{Ca} -CaV coupling, may abolish bursting activity. Our simulations showed that even the simplification given by Eq. 29 provided reliable results (Figure 3E-G). Similar conclusions hold for the β -cell model (see Figure S7). Interestingly, this was not the case in the neuronal model (20) (Figure S6), likely because of the shorter neuronal AP being more sensitive to the kinetics of BK_{Ca} activation.

A general strategy to distinguish between different configurations of the BK_{Ca} -CaV complex could be to, first, estimate the maximal whole-cell BK_{Ca} conductance, for example by depolarizations to highly positive voltages to activate BK_{Ca} channels independently of CaV activity (16), and, then, to fit I-V curves obtained from voltage-clamp depolarizations (37, 40) using the expressions presented here.

In summary, we have presented a concise Hodgkin-Huxley-type model of BK_{Ca} currents that take into account local control in BK_{Ca} -CaV complexes with different stoichiometries. Our model should be useful for whole-cell simulations of electrical activity in neurons and other excitable cells. The approach should be relatively straight-forward to apply to other ion channel complexes, e.g., the Cav3-Kv4 complex (45).

Authors' contributions

All authors performed research, prepared SM, revised the paper and approved the final version. F.M., A.T. and M.G.P. prepared figures. F.M. developed methods. M.G.P. conceived research and wrote the paper.

Acknowledgements

We have no competing interests. We thank Carles Rovira, University of Barcelona, for useful discussions during early phases of the work.

References

1. Hodgkin, A. L., and A. F. Huxley, 1952. A quantitative description of membrane current and its application to conduction and excitation in nerve. *J Physiol* 117:500–44.
2. Berkefeld, H., B. Fakler, and U. Schulte, 2010. Ca²⁺-activated K⁺ channels: from protein complexes to function. *Physiol Rev* 90:1437–59.
3. Pallotta, B. S., K. L. Magleby, and J. N. Barrett, 1981. Single channel recordings of Ca²⁺-activated K⁺ currents in rat muscle cell culture. *Nature* 293:471–4.
4. Barrett, J. N., K. L. Magleby, and B. S. Pallotta, 1982. Properties of single calcium-activated potassium channels in cultured rat muscle. *J Physiol* 331:211–30.
5. Cox, D. H., J. Cui, and R. W. Aldrich, 1997. Allosteric gating of a large conductance Ca-activated K⁺ channel. *J Gen Physiol* 110:257–81.
6. Latorre, R., and S. Brauchi, 2006. Large conductance Ca²⁺-activated K⁺ (BK) channel: activation by Ca²⁺ and voltage. *Biol Res* 39:385–401.
7. Grunnet, M., and W. A. Kaufmann, 2004. Coassembly of big conductance Ca²⁺-activated K⁺ channels and L-type voltage-gated Ca²⁺ channels in rat brain. *J Biol Chem* 279:36445–53.
8. Berkefeld, H., C. A. Sailer, W. Bildl, V. Rohde, J.-O. Thumfart, S. Eble, N. Klugbauer, E. Reisinger, J. Bischofberger, D. Oliver, H.-G. Knaus, U. Schulte, and B. Fakler, 2006. BKCa-Cav channel complexes mediate rapid and localized Ca²⁺-activated K⁺ signaling. *Science* 314:615–20.
9. Müller, A., M. Kukley, M. Uebachs, H. Beck, and D. Dietrich, 2007. Nanodomains of single Ca²⁺ channels contribute to action potential repolarization in cortical neurons. *J Neurosci* 27:483–95.
10. Rehak, R., T. M. Bartoletti, J. D. T. Engbers, G. Berecki, R. W. Turner, and G. W. Zamponi, 2013. Low voltage activation of KCa1.1 current by Cav3-KCa1.1 complexes. *PLoS One* 8:e61844.
11. Suzuki, Y., H. Yamamura, S. Ohya, and Y. Imaizumi, 2013. Caveolin-1 facilitates the direct coupling between large conductance Ca²⁺-activated K⁺ (BKCa) and Cav1.2 Ca²⁺ channels and their clustering to regulate membrane excitability in vascular myocytes. *J Biol Chem* 288:36750–61.
12. Chad, J. E., and R. Eckert, 1984. Calcium domains associated with individual channels can account for anomalous voltage relations of CA-dependent responses. *Biophys J* 45:993–9.
13. Simon, S. M., and R. R. Llinás, 1985. Compartmentalization of the submembrane calcium activity during calcium influx and its significance in transmitter release. *Biophys J* 48:485–498. [http://dx.doi.org/10.1016/S0006-3495\(85\)83804-2](http://dx.doi.org/10.1016/S0006-3495(85)83804-2).
14. Neher, E., 1998. Vesicle pools and Ca²⁺ microdomains: new tools for understanding their roles in neurotransmitter release. *Neuron* 20:389–399.

15. Fakler, B., and J. P. Adelman, 2008. Control of K(Ca) channels by calcium nano/microdomains. *Neuron* 59:873–881. <http://dx.doi.org/10.1016/j.neuron.2008.09.001>.
16. Berkefeld, H., and B. Fakler, 2013. Ligand-gating by Ca²⁺ is rate limiting for physiological operation of BK(Ca) channels. *J Neurosci* 33:7358–67.
17. Cox, D. H., 2014. Modeling a Ca(2+) channel/BKCa channel complex at the single-complex level. *Biophys J* 107:2797–814.
18. Stanley, D. A., B. L. Bardakjian, M. L. Spano, and W. L. Ditto, 2011. Stochastic amplification of calcium-activated potassium currents in Ca²⁺ microdomains. *J Comput Neurosci* 31:647–66.
19. Anwar, H., I. Hepburn, H. Nedelescu, W. Chen, and E. De Schutter, 2013. Stochastic calcium mechanisms cause dendritic calcium spike variability. *J Neurosci* 33:15848–67.
20. Roper, P., J. Callaway, T. Shevchenko, R. Teruyama, and W. Armstrong, 2003. AHP's, HAP's and DAP's: how potassium currents regulate the excitability of rat supraoptic neurones. *J Comput Neurosci* 15:367–89.
21. Tabak, J., N. Toporikova, M. E. Freeman, and R. Bertram, 2007. Low dose of dopamine may stimulate prolactin secretion by increasing fast potassium currents. *J Comput Neurosci* 22:211–22.
22. Pedersen, M. G., 2010. A biophysical model of electrical activity in human β -cells. *Biophys J* 99:3200–3207. <http://dx.doi.org/10.1016/j.bpj.2010.09.004>.
23. Riz, M., M. Braun, and M. G. Pedersen, 2014. Mathematical modeling of heterogeneous electrophysiological responses in human β -cells. *PLoS Comput Biol* 10:e1003389.
24. Khaliq, Z. M., N. W. Gouwens, and I. M. Raman, 2003. The contribution of resurgent sodium current to high-frequency firing in Purkinje neurons: an experimental and modeling study. *J Neurosci* 23:4899–912.
25. Jaffe, D. B., B. Wang, and R. Brenner, 2011. Shaping of action potentials by type I and type II large-conductance Ca²⁺-activated K⁺ channels. *Neuroscience* 192:205–18.
26. Anwar, H., S. Hong, and E. De Schutter, 2012. Controlling Ca²⁺-activated K⁺ channels with models of Ca²⁺ buffering in Purkinje cells. *Cerebellum* 11:681–93.
27. Sherman, A., J. Keizer, and J. Rinzel, 1990. Domain model for Ca²⁺(+)-inactivation of Ca²⁺ channels at low channel density. *Biophys J* 58:985–995. [http://dx.doi.org/10.1016/S0006-3495\(90\)82443-7](http://dx.doi.org/10.1016/S0006-3495(90)82443-7).
28. Hinch, R., J. L. Greenstein, A. J. Tanskanen, L. Xu, and R. L. Winslow, 2004. A simplified local control model of calcium-induced calcium release in cardiac ventricular myocytes. *Biophys J* 87:3723–36.
29. Greenstein, J. L., R. Hinch, and R. L. Winslow, 2006. Mechanisms of excitation-contraction coupling in an integrative model of the cardiac ventricular myocyte. *Biophys J* 90:77–91.

30. Williams, G. S. B., M. A. Huertas, E. A. Sobie, M. S. Jafri, and G. D. Smith, 2007. A probability density approach to modeling local control of calcium-induced calcium release in cardiac myocytes. *Biophys J* 92:2311–28.
31. Lobo, F. G., and D. E. Goldberg, 1997. Decision making in a hybrid genetic algorithm. *In* IEEE International Conference on Evolutionary Computation, 1997. IEEE, 121–125.
32. Fleming, P. J., and R. C. Purshouse, 2002. Evolutionary algorithms in control systems engineering: a survey. *Control engineering practice* 10:1223–1241.
33. Neher, E., 1998. Usefulness and limitations of linear approximations to the understanding of Ca^{++} signals. *Cell Calcium* 24:345–57.
34. Marcantoni, A., D. H. F. Vandael, S. Mahapatra, V. Carabelli, M. J. Sinnegger-Brauns, J. Striessnig, and E. Carbone, 2010. Loss of Cav1.3 channels reveals the critical role of L-type and BK channel coupling in pacemaking mouse adrenal chromaffin cells. *J Neurosci* 30:491–504.
35. Buchholz, P., J. Kriege, and I. Felko, 2014. Input modeling with phase-type distributions and Markov models. Springer Briefs in Mathematics. Springer. <http://dx.doi.org/10.1007/978-3-319-06674-5>.
36. Segel, L. A., and M. Slemrod, 1989. The quasi steady-state assumption: a case study in perturbation. *SIAM Rev.* 31:446–477.
37. Berkefeld, H., and B. Fakler, 2008. Repolarizing responses of BKCa-Cav complexes are distinctly shaped by their Cav subunits. *J Neurosci* 28:8238–45.
38. Storm, J. F., 1987. Action potential repolarization and a fast after-hyperpolarization in rat hippocampal pyramidal cells. *J Physiol* 385:733–59.
39. Joux, N., V. Chevalyere, G. Alonso, L. Boissin-Agasse, F. C. Moos, M. G. Desarménien, and N. Hussy, 2001. High voltage-activated Ca^{2+} currents in rat supraoptic neurones: biophysical properties and expression of the various channel alpha1 subunits. *J Neuroendocrinol* 13:638–49.
40. Braun, M., R. Ramracheya, M. Bengtsson, Q. Zhang, J. Karanauskaite, C. Partridge, P. R. Johnson, and P. Rorsman, 2008. Voltage-gated ion channels in human pancreatic beta-cells: electrophysiological characterization and role in insulin secretion. *Diabetes* 57:1618–1628. <http://dx.doi.org/10.2337/db07-0991>.
41. Houamed, K. M., I. R. Sweet, and L. S. Satin, 2010. BK channels mediate a novel ionic mechanism that regulates glucose-dependent electrical activity and insulin secretion in mouse pancreatic β -cells. *J Physiol* 588:3511–23.
42. Stojilkovic, S. S., H. Zemkova, and F. Van Goor, 2005. Biophysical basis of pituitary cell type-specific Ca^{2+} signaling-secretion coupling. *Trends Endocrinol Metab* 16:152–9.
43. Tagliavini, A., J. Tabak, R. Bertram, and M. G. Pedersen, 2016. Is bursting more effective than spiking in evoking pituitary hormone secretion? A spatiotemporal simulation study of calcium and granule dynamics. *Am J Physiol Endocrinol Metab* 310:E515–25.

44. Sun, X.-P., B. Yazejian, and A. D. Grinnell, 2004. Electrophysiological properties of BK channels in *Xenopus* motor nerve terminals. *J Physiol* 557:207–28.
45. Anderson, D., W. H. Mehafeey, M. Iftinca, R. Rehak, J. D. T. Engbers, S. Hameed, G. W. Zamponi, and R. W. Turner, 2010. Regulation of neuronal activity by Cav3-Kv4 channel signaling complexes. *Nat Neurosci* 13:333–7.

Supporting Material

A single .pdf file including the supporting text, figures and tables.

Supporting File S1

A zipped folder containing the MATLAB code for generating the results presented in the main text and Supporting Material.